Mring: Contactless MR/AR Extended Input Method based on Magnetic Signal

CHAO LIU, Ocean University of China, China
YIPENG LIU, Ocean University of China, China
FENG HONG, Ocean University of China, China
ZHONGWEN GUO, Ocean University of China, China
JIGUO YU, University of Electronic Science and Technology of China, China
FENG LI*, Shandong University, China

In recent years, the rapid rise of Mixed Reality (MR) and Augmented Reality (AR) technologies has transformed digital interactions and immersive experiences, as evidenced by their widespread adoption in AR glasses, MR headsets, and mobile AR applications. However, integrating MR and AR into everyday life also presents unique problems, particularly concerning user interactions within limited visual fields and discomfort caused by prolonged arm elevation. To address these challenges, our research introduces an innovative input device utilizing common wearable device magnetometer sensors and a strong magnet as input controls. We employ innovative methods to eliminate environmental magnetic field and soft magnetic offset, achieving trajectory restoration with an error margin of 5.23 mm through machine learning and trajectory smoothing algorithms. This enables our input device to interact with MR and AR devices beyond the user's visual range, expanding operational space, and enhancing usability.

CCS Concepts: • **Human-centered computing → HCI theory, concepts and models**; **Ubiquitous and mobile computing systems and tools**.

Additional Key Words and Phrases: Magnetic Sensing, Wireless Sensing, Localization, Soft iron calibration, Model Distillation

ACM Reference Format:
Chao Liu, Yipeng Liu, Feng Hong, Zhongwen Guo, Jiguo Yu, and Feng Li. 2025. Mring: Contactless MR/AR Extended Input Method based on Magnetic Signal. *ACM Trans. Sensor Netw.* 1, 1, Article 1 (January 2025), 26 pages. https://doi.org/10.1145/3592612

1 INTRODUCTION

In recent years, Mixed Reality (MR) and Augmented Reality (AR) technologies have experienced an unprecedented surge in popularity, fundamentally altering how we engage with digital information and immersive experiences. The widespread adoption of MR and AR devices, such as AR glasses, MR headsets, and mobile AR applications, underscores the growing interest and investment in these transformative technologies. These devices seamlessly integrate virtual elements into the

*Corresponding author

Authors' addresses: Chao Liu, liuchao@ouc.edu.cn, Ocean University of China, Qingdao, Shandong, China; Yipeng Liu, Ocean University of China, China, liuyipeng6901@stu.ouc.edu.cn; Feng Hong, Ocean University of China, China, hongfeng@ouc.edu.cn; Zhongwen Guo, Ocean University of China, China, guozhw@ouc.edu.cn; Jiguo Yu, University of Electronic Science and Technology of China, China, jiguoyu@sina.com; Feng Li, Shandong University, China, fli@sdu.edu.cn.

1550-4859/2025/1-ART1 $15.00
https://doi.org/10.1145/3592612

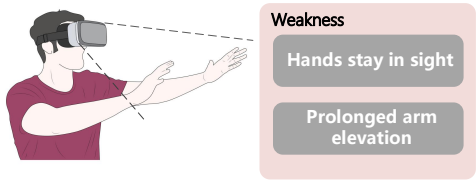

Fig. 1. Manipulating MR with Limited Line of Sight

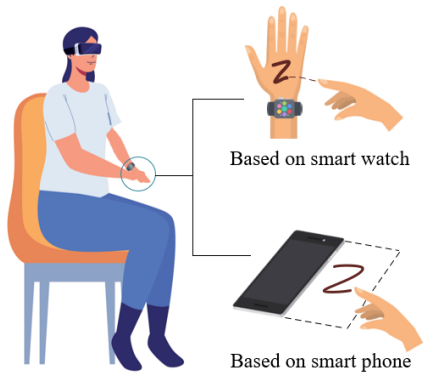

Fig. 2. Manipulating MR Beyond Line of Sight

Table 1. Comparison of Different Camera Types and Prices

Model	Camera Type	Downward Camera	Price(USD)
Apple Vision Pro	Infrared cameras	Yes	$3,499
PICO 4 VR	High-resolution color and tracking cameras	No	$657
XREAL AIR 2 ULTRA	Forward camera array	No	$559
Rokid Air+Station	Forward camera array	No	$252

real world, providing users with a dynamic and interactive environment. From enriching gaming experiences to revolutionizing education and training, MR and AR have found diverse applications in various industries.

Despite significant advancements in MR and AR technologies, as depicted in Figure 1, gesture-based interactions between users and devices still present considerable challenges. A primary issue arises from the limited field of view in many devices, which affects their ability to capture hand movements effectively. For instance, as indicated in Table 1, only Apple's Vision Pro is equipped with downward-facing cameras that allow for tracking hands below the user's line of sight. In contrast, popular devices such as the PICO 4 VR, XREAL AIR 2 ULTRA, and Rokid Air+Station are restricted to forward-facing cameras, severely limiting their ability to capture interactions outside the immediate visual field.

This constraint on visual coverage can result in decreased accuracy and fluidity of interactions, especially in scenarios requiring precise hand movements below eye level, such as manipulating objects on a surface or performing detailed gesture-based tasks. Over time, these limitations not only hinder seamless interaction but also lead to physical discomfort, such as arm fatigue from prolonged elevation when interacting with the virtual environment. This results in a less immersive experience and reduces the practicality of the technology for long-term use. Given these challenges, there is an urgent need for more advanced interaction techniques that extend beyond the confines of the current visual tracking systems. Addressing these limitations will improve both usability and user comfort by allowing for more natural hand movements and reducing physical strain during extended interaction sessions in MR and AR environments.

Numerous previous studies have explored gesture tracking and recognition using acoustic and RF-based techniques (with relevant references). However, both approaches have significant limitations. Research such as EchoTrack[29] and VoLoc[4] has utilized acoustic signals, leveraging echo effects for human positioning and identification. These methods are highly sensitive to ambient noise, which can lead to significant distortion in noisy environments, making them unsuitable for tasks requiring high precision. As for RF-based works, such as WiGesture[9] and CrossGR[11], although RF signals have a greater sensing range compared to acoustic waves, they suffer from issues such as signal attenuation, reflection, and low resolution in distance perception. These factors result in reduced positioning accuracy and reliability, which fail to meet the precision demands of MR and AR systems. Additionally, RF signals are susceptible to interference from other RF sources, further compromising their effectiveness in dynamic or cluttered environments.

In contrast, magnetic signals are less variant and more stable compared to RF and acoustic signals. They are less susceptible to external environmental factors such as noise and interference, ensuring stable and accurate tracking. Additionally, magnetic signals maintain their integrity even in complex environments, providing consistent and reliable data for precise tasks. Moreover, the use of magnetic sensing often comes at a lower cost compared to other technologies, adding an economical advantage. This combination of effectiveness, reliability, and cost-efficiency makes magnetic signals a novel and effective choice for meeting the demands of MR and AR interactions, where stability and adaptability are crucial.

As a solution, we propose a system called Mring, which is illustrated in Figure 2. This system utilizes a wearable magnet (Mring) in combination with magnetometer sensors integrated into smartphones or smartwatches. This approach leverages the benefits of stationary device stability, while also offering an ergonomic and energy-efficient design for precise control during interactive tasks like handwriting and sketching in MR/AR environments. This system utilizes a wearable magnet on a ring and integrates magnetometer sensors within stationary devices such as smartphones and smartwatches. This allows for precise interactions, even when the device is outside the user's direct line of sight, by capturing subtle hand movements. The stationary nature of the devices supports natural user behavior, where stabilizing the device during tasks like writing and drawing allows for better focus and minimizes physical strain. Moreover, this approach aligns with the real-world expectations of Human-Computer Interaction, where users typically stabilize their devices to concentrate fully on fine-tuned movements. This principle is respected in our design, ensuring the device remains stationary to improve usability and satisfaction. By avoiding the need for users to hold their arms up for extended periods, our system allows for a more comfortable and healthy sitting posture during prolonged interactions. In practical terms, imagine a user sitting at a desk with their smartphone on the table, interacting through the Mring. The smartphone, while stationary, effectively tracks the magnetic signals from the ring, enabling precise tracking of the user's hand movements. This setup not only ensures stable signal capture and accurate interaction but also minimizes power consumption and removes the requirement for external hardware, making it both cost-effective and suitable for everyday use.

By focusing on these key aspects of device stability, user ergonomics, and seamless integration with existing technology, the Mring system enhances precision and control in MR/AR environments, supporting a fluid and natural interaction experience that is both intuitive and satisfying.

To achieve our research objectives, we encountered several challenges:

Electromagnetic Interference: Compared to traditional magnetic environments, the simultaneous use of AR and MR devices results in significant electromagnetic interference, leading to substantial data disturbances. Additionally, the surrounding soft magnetic effects have a considerable impact, causing the magnetic background data to be nonlinear and unstable.

User/Scene Adaptation: Dealing with diverse scenarios and user usage, particularly on the smartwatch platform, requires special adaptation due to computational constraints. Additionally, specialized transfer learning is necessary for different environments and user scenarios to ensure the system performs well in various situations. Personalized adaptation and specialized transfer learning require additional time and resources, but are crucial for improving the overall performance and user experience of the system.

Our research tackles significant challenges in the realm of MR and AR interactions. Firstly, we combat electromagnetic interference by employing noise filtering and stabilizing the background magnetic field through linear methods. We then process data using a magnetic dipole model and train neural networks to handle soft magnetic offsets. Additionally, our system achieves an impressive 5.23 mm precision level, ensuring accurate user trajectory reconstruction even in areas with weak magnetic signals. This precision, coupled with our trajectory smoothing algorithm, enhances the overall user experience. Furthermore, we address the diversity of scenarios by developing a comprehensive calibration approach for different users and environments. For smartwatches, we optimize computational costs by distilling models from smartphones while maintaining high accuracy levels. This integrated approach allows us to overcome key challenges, delivering a robust and adaptable system for MR and AR technologies.

Specifcally, our contributions include:

- We propose a novel interaction method for application in MR and AR devices, utilizing low-cost permanent magnets as input devices. This method involves collecting and processing signals for positioning and trajectory reconstruction, enabling operation of MR and AR devices outside the line of sight.
- We introduce an innovative approach to address soft magnetic offset, employing a magnetic dipole model for initial processing and further refinement using neural networks.
- Our trajectory reconstruction average error is approximately 5.23mm. On the smartphone platform, the average error can be reduced to around 4.55mm, while on the smartwatch platform, it is approximately 7.02mm.
- Our localization and trajectory tracking services are implemented across multiple platforms, including smartphones and smartwatches. We also optimized the model for smartwatches by performing model distillation to overcome computational limitations, the error increased by only about 1mm compared to the original model.

The remainder of this paper is organized as follows: In Section II, we present related work. Section III outlines the overall design of our system. In Section IV, we delve into our research, providing a detailed analysis of signal processing, soft magnetic offset correction, localization recognition, user adaptation, and trajectory reconstruction algorithms. Section V discusses further optimization of the system. Section VI explores the limitations of our system. Finally, Section VII concludes this paper.

2 RELATED WORK

Modern technology has made hand tracking essential in many areas like virtual reality, healthcare, intelligent interaction, and industrial production[18, 30, 40, 41]. This section will review different methods of hand tracking, with a particular focus on the applications and advancements in utilizing acoustic signals, RF signals, and magnetic signals.

2.1 MR/AR Applications

Recently, with the continuous maturation of MR (Mixed Reality) and AR (Augmented Reality) devices, various practical applications based on MR and AR have emerged one after another. This

has allowed head-mounted devices to play a significant role in multiple fields. In the industrial sector, Anthony Paul Franze et. al [8] design more efficient fabrication and assembly practices using MR/AR devices; In the realm of creative work, MR has also played a significant role. Xiangwen Xiong et. al [33] proposed a method, which can eliminates the gravity and weight of the devices and components that mounted and dressed in the human body, but also come true the interacting scenes and following behaviors and actuations in story lines. Virtual Makerspaces [19] present a mixed-reality system for remote collaborations, where collaborators can discuss, explore, create and learn about 3D physical objects. Additionally, other technology [7, 10, 16, 20, 23] have expanded the infinite possibilities of MR/AR devices in other areas, such as reading, medicine, interpersonal communication, and more.

2.2 Hand Tracking Applications

2.2.1 Acoustic-based. Acoustic-based hand tracking is a prevalent method for estimating hand positions and gestures by capturing sound or ultrasonic signals through microphones or ultrasonic sensors[26, 27, 34]. Strata[36] introduces a novel approach by utilizing a mobile device (e.g., smartphone) that transmits known audio signals at inaudible frequencies and analyzes the signal reflected by the moving finger to accurately track its location. LLAP [28] and FingerIO[14]represent significant advancements in acoustic signal-based tracking by using the reflected audio signals from a mobile phone for finger movement detection. LLAP employs a phase-based tracking system, enhancing accuracy and reducing the complexity involved in the signal processing chain. Conversely, FingerIO utilizes OFDM symbol-based movement detection, which provides robustness against noise and improves the precision of near-field finger tracking. While these systems achieve high precision in gesture tracking, their performance can be limited in complex environments such as underwater settings, where signal degradation is prominent. Acoustic signal-based hand tracking, as seen in methods like Strata, LLAP, and FingerIO, faces significant limitations. These systems are prone to noise interference, which can distort tracking accuracy in noisy environments. Additionally, they pose privacy risks by potentially capturing sensitive audio. Physical barriers also hinder their effectiveness, as acoustic signals have limited penetration capabilities.

Mring distinguishes itself by utilizing magnetic signals, which provide stable and accurate tracking, even in noisy or dynamically changing environments. Unlike acoustic signals that are often compromised by noise and other environmental factors, Mring's magnetic tracking maintains integrity and reliability. This stability is crucial for ensuring accurate tracking data in complex settings, where acoustic methods may struggle with interference and distortions. As a result, Mring consistently delivers reliable data for precise tasks, demonstrating its robustness and adaptability.

2.2.2 RF-based. In our review of WiFi-based gesture recognition and tracking methods, we've identified several inherent limitations associated with RF technologies, as highlighted in key studies like WiSee [17], WiTrack [2]. These systems, while leveraging RF signals to cover expansive areas, often encounter significant challenges such as attenuation and reflection, particularly in complex or cluttered environments. This degradation can critically impair positioning accuracy and reliability, which are essential for precise tracking tasks. Moreover, these RF signals are highly susceptible to interference from other RF sources, further compromising their tracking accuracy. Additionally, studies such as mTrack [31] and Soli [24] employ 60 GHz signals that demonstrate reduced interference and promise enhanced precision. However, they also reveal critical limitations related to the necessity for substantial additional hardware, which escalates costs and complicates deployment. These systems also grapple with bandwidth limitations, a notable drawback of RF technologies that can restrict data transmission rates, adversely impacting the responsiveness and accuracy of the tracking system.

In contrast, Mring achieves exceptional stability through the use of advanced noise reduction and signal processing techniques. It utilizes magnetic signals, which are free from the bandwidth constraints typical of RF signals and offer superior security. Leveraging the magnetometers already present in smartphones, Mring eliminates the need for additional hardware, enhancing its cost-effectiveness. The integration of these advanced technologies allows Mring to adapt to a variety of environments, enhancing its practicality and effectiveness in MR and AR applications.

2.3 Magnetic Tracking

2.3.1 Permanent Magnets-based. In recent studies, several innovative methods for utilizing magnetic fields in tracking systems have been developed, each demonstrating unique capabilities but also exhibiting limitations in flexibility and precision. MagneTrack[1] enables continuous and simultaneous 1-DOF tracking of two magnets by employing a magnetic field separation method. FieldSweep [13] offers a 2D tracking system on a plane using permanent magnets and a smartphone. Additionally, input techniques to the surface around a smartphone use magnets attached to a stylus for graphical matching. SynchroWatch [21] recognizes one-handed synchronous smartwatch gestures through correlation and magnetic sensing. TRing [35] introduces a finger-worn input device for instant and customizable interactions with objects. Lastly, MagX [5] presents an untethered hand tracking system utilizing passive magnets and a novel magnetic sensing platform. While these advancements highlight the diverse applications and capabilities of magnetic-based tracking technologies, they often lack the flexibility and precision needed for more dynamic and detailed interaction scenarios, which can limit their practical usability in complex environments.

Moreover, in the realm of utilizing permanent magnets for tracking, compared to the aforementioned endeavors, there is a greater emphasis on single magnetometry. However, Mring offers higher precision and greater flexibility compared to previous methods. Instead of relying on fixed pattern matching, it utilizes a combination of recognition-based positioning and trajectory optimization algorithms. This enables the restoration of user inputs. Moreover, Mring utilizes only a single magnet and the magnetometer on a smartwatch, eliminating the need for additional hardware. This not only further reduces the cost but also enhances the user experience.

2.3.2 Electromagnets-based. In addition, there has been a development in utilizing electromagnets for magnetic sensing. MagSound [25] leverages the electromagnetic effects of earphones to enhance tracking and acoustic sensing in Commercial-Off-The-Shelf (COTS) earphones. Magnetips [12] integrates fingertip tracking and haptic feedback for around-device interaction. Aura [15] presents an inside-out electromagnetic 6-DoF tracking system designed for handheld controllers. Make It Trackable [22] introduces an instant magnetic tracking system using coil-free tiny trackers. Finally, Finexus [6] enables precise motion tracking of multiple fingertips through magnetic sensing. In terms of hand positioning and recognition, electromagnetic tracking necessitates the use of additional equipment such as coils, which is less convenient compared to Mring.

3 SYSTEM OVERVIEW

Our system primarily relies on magnetic sensing technology and is divided into three progressive stages: magnetic signal processing, user and environment adaptation, and trajectory smoothing and reconstruction. The process is illustrated in Figure 3. The initial stage focuses on processing the magnetic signals received by the smartwatch, with an emphasis on mitigating environmental interference. In the second stage, parameters are calibrated in a specific manner, and data on the user and environment are collected to address their impact on the magnetic signals. Finally, the processed data is used to train complex neural networks to obtain the user's input coordinates, which are then further refined through a trajectory smoothing algorithm to minimize errors.

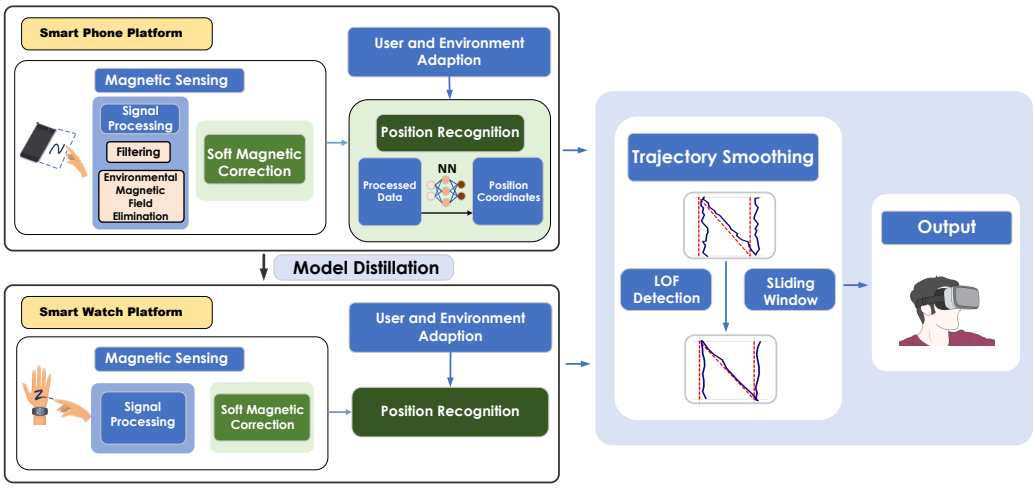

Fig. 3. System Overview of Mring

Magnetic Signal Processing: In this phase, we process the magnetic signals received by the smartwatch to remove environmental influences. Firstly, we use filtering techniques to reduce noise in the received data. Then, we address the effects of the ambient magnetic field, which mainly consist of two components: the Earth's magnetic field and magnetization effects caused by nearby metals or electronic components due to the presence of magnets, which significantly affect the magnetic data.

Magnetization effects can be categorized into two types: hard magnetic effects and soft magnetic effects. Hard magnetic effects are stable over time and can be eliminated together with the Earth's magnetic field. We employ a sliding-window approach to calculate the real-time ambient background magnetic field and remove it. However, soft magnetic effects are unstable and nonlinear, closely related to the properties of materials. Therefore, we opt for training a neural network to accurately remove the soft magnetic offset.

Additionally, it's important to note that the choice of neural network for handling soft magnetic effects involves considerations such as training data, model architecture, and validation methods to ensure effective removal of soft magnetic distortions.

User and Environment Adaptation: Due to the diverse scenarios of use of the smartwatch, we employ transfer learning techniques to adapt to different environments and users. When users enter a new environment, specific actions are required to gather new features related to the environment and the users. This adaptation process only requires a small number of user samples to achieve effective adaptation.

Positioning Recognition: In this phase, we utilize a sophisticated neural network comprising two distinct sections, each with six hidden layers, to train the conversion of magnetic signals into positioning coordinates. Given that the target usage scenario is a smartwatch, we also perform knowledge distillation on the model to ensure smooth operation on the smartwatch chip. Finally, we employ trajectory smoothing algorithms to concatenate the identified points and obtain the final user input result.

It's worth noting that the choice of neural network architecture, training techniques such as knowledge distillation, and the integration with smartwatch hardware constraints are critical aspects of this phase's implementation for accurate positioning and user-friendly performance.

4 MAGNETIC SENSING

In this section, we explore the key aspects of magnetic sensing, a critical component of our study. This chapter focuses on the design and calibration of a magnetic sensing system for smartwatches, using permanent magnets for interaction. We address the challenges in signal processing, particularly in adapting to environmental magnetic fields and reducing noise, to enhance the accuracy and reliability of the system. Furthermore, we discuss the development of specialized models for soft magnetic correction and position recognition. These models, developed through deep learning techniques, aim to refine the system's precision in detecting positions. This overview provides a foundation for the detailed discussions that follow, outlining our approach to improving magnetic sensing technology.

4.1 Signal Processing

4.1.1 Noise Reduction Processing. In the noise reduction process of signal processing, we implement the Kalman filter, a sophisticated algorithm well-suited for handling data with inherent uncertainties. The core of our magnetic sensing system involves interpreting magnetic force vectors, which are expressed as three-dimensional arrays (x, y, z). Under standard conditions, these vectors tend to change smoothly over time. However, the environmental magnetic field can experience abrupt fluctuations, which introduce significant noise into the magnetic data.

The Kalman filter [32] is particularly effective in this scenario. Its primary function is to smooth out the data by providing a statistically optimal estimate of the magnetic vector state. By doing so, it effectively eliminates the noise caused by sudden changes in the environmental magnetic field. This ensures the integrity and reliability of the magnetic signal, especially in dynamic environments. Consequently, the application of the Kalman filter is crucial for maintaining the precision of our magnetic sensing system, as it allows for a more accurate interpretation of the magnetic field variations, which is critical for the system's overall performance.

4.1.2 Environmental Magnetic Field Elimination. In the process of environmental magnetic field elimination, our approach relies on the stability of the magnetic field in the surrounding environment. The initial step involves calculating the cosine similarity of magnetic field vectors to assess changes in the environmental magnetic field. This is achieved by comparing the cosine similarity of the current magnetic vector with the previous one.

The cosine similarity, denoted as CS, is defined as:

$$\mathrm{CS} = \frac{\mathbf{V}_c \cdot \mathbf{V}_p}{\|\mathbf{V}_c\| \|\mathbf{V}_p\|}, \tag{1}$$

where $\mathbf{V}_c$ and $\mathbf{V}_p$ represent the current and previous magnetic vectors, respectively. This similarity measure is then compared with a predefined threshold to determine the stability of the environmental magnetic field. If the field is deemed stable, the system continues to record magnetic vectors until instability is detected.

Once the environmental magnetic field is considered unstable, the most recent 20 recorded vectors are analyzed. For each component of the magnetic vector (x, y, and z), the mean is calculated by

$$\mathbf{V}_x = \frac{1}{n}\sum_{i=1}^{n} V_{x,i}, \tag{2}$$

$$\mathbf{V}_y = \frac{1}{n}\sum_{i=1}^{n} V_{y,i}, \tag{3}$$

$$\mathbf{V}_z = \frac{1}{n}\sum_{i=1}^{n} V_{z,i}, \tag{4}$$

where $\mathbf{V}_x$, $\mathbf{V}_y$, and $\mathbf{V}_z$ represent the mean values of the components x, y, and z of the magnetic vector, respectively, and n is the number of vectors considered (in this case 20).

These mean values are then used to adjust the magnetic vector data, effectively eliminating the influence of the environmental magnetic field. This adjustment is crucial for ensuring the accuracy of subsequent signal processing and positioning tasks.

4.2 Modeling for Positioning and Magnetic Correction

Delving into the intricacies of model training, our exploration begins with the development of a specialized model tailored to address soft magnetic offsets. The paramount goal is to rectify data, thereby augmenting the overall accuracy of our experimental results. Following this, we investigate target localization recognition based on the refined data set. Ultimately, through the application of model transfer techniques, we endeavor to ensure the adaptability of our model across diverse environmental contexts.

4.2.1 Soft Magnetic Correction Model Training. Magnetic interference is a critical factor to consider in positioning and recognition systems, as it can significantly affect accuracy[39]. To address this, it is important to categorize and understand the different sources of interference. Magnetic interference can be divided into two main types: Hard Magnetic Interference and Soft Magnetic Interference.

Hard Magnetic Interference is caused by materials such as Neodymium-Iron-Boron, which are commonly used in refrigerator magnets and headphones, and Ferrite, found in household speakers, radios, and TV antennas. These materials generate strong, stable magnetic fields that can distort positioning accuracy if not accounted for. In contrast, Soft Magnetic Interference arises from materials like Silicon Steel (used in phone chargers and power adapters), Soft Iron (used in electromagnetic door locks and speakers), and Nickel-Iron Alloys (found in computer hard drives and televisions). These materials produce more variable magnetic fields that are sensitive to external factors, making them more challenging to manage in real-time systems.

Moreover, the challenge of measuring and mitigating these effects is compounded by the non-linearity of magnetic materials, which is illustrated by the hysteresis curve. This nonlinearity makes it difficult to use a unified model for calculating magnetic effects, particularly when dealing with soft magnetic interference from common appliances. By categorizing the sources of magnetic interference and understanding their behavior, we can better design systems that mitigate their impact and improve overall accuracy.

The initial data pre-processing involves the application of the magnetic force formula to mitigate soft magnetic offsets induced by magnetic influences [37]. Initially, the magnetic field strength (H)

is calculated using the magnetic dipole formula:

$$H = \frac{1}{(4\pi)} \frac{m}{r^3}, \tag{5}$$

where H represents the magnetic field strength at the calculated position, m is the magnetic moment, r is the distance, and other variables are appropriately defined. Subsequently, considering ideal magnetometer conditions, the measured magnetic field which is written as Mag is obtained as the projection of Earth's magnetic induction in the body coordinate system, given by:

$$Mag = D \cdot Mag_{ec}, \tag{6}$$

where D represents the matrix describing the orientation transformation from the Earth coordinate system to the body coordinate system. Mag_{ec} denotes the magnetic induction strength in the Earth coordinate system, projecting the magnetic field within that frame of reference.

Further, the relationship between magnetic flux density (B) and magnetic field (H) is expressed by:

$$B = \mu \cdot H = \mu_0 \cdot \mu_r \cdot H, \tag{7}$$

By simultaneously solving the above equations, the following formula can be derived:

$$B = \mu_0^{1/2} \cdot \mu_r \cdot (\mu_0 - m \cdot B_r)^{3/2} \cdot r \cdot (t^{-a}), \tag{8}$$

where μ_0 is the permeability of free space, μ_r is the relative permeability, m is the magnetic moment, B_r is the remanence, r is the distance, t is time, and a is an exponent that captures the diminishing effect of soft magnetic offsets over time. The term t^{-a} signifies the decay of soft magnetic effects as time progresses.

Through preliminary experiments, we first conducted trials in a non-magnetic environment, devoid of any materials that could induce soft magnetic effects, to establish baseline data collection. Subsequently, we replicated these experiments in a conventional environment, where typical ambient magnetic disturbances are present, to gather comparative data. Each experimental setting involved the collection of data over ten sessions.

For our analysis, we paired one set of data from the non-magnetic environment with one from the conventional environment, calculating the cosine similarity for each pair. The process was repeated for ten such pairs, and the average cosine similarity across all pairs was found to be approximately 0.98. This high level of similarity suggests that while the soft magnetic effects can cause noticeable disturbances at the edges of the experimental area, particularly with the millimeter-level precision required, the overall direction of the magnetic force vectors remains largely unaffected. This consistency underscores the need to determine a magnitude factor to accurately recover the original true data from the measurements obtained under typical environmental conditions.

Utilizing this insight, the formula provides a foundation for determining the key variables influencing soft magnetic offsets. By isolating environmental constants and focusing on the remaining variables such as magnetic moment, distance, and time, we can use machine learning techniques to fit the impact of these parameters. This approach allows us to preliminary estimate the effect of soft magnetic offsets and progressively refine the model to reduce their impact on the system, thereby improving the accuracy of magnetic readings.

In our pursuit of an effective soft magnetic offset correction model, we established a universal standard for assessing accuracy. This standard relies on the Euclidean Distance metric, which quantifies the spatial difference between the predicted and true data vectors. By comparing the Euclidean Distance to a predefined threshold (k), we can evaluate the success of the calibration process. Building on the previously identified variables influencing soft magnetic offsets, our model adjusts these parameters through machine learning techniques to minimize the Euclidean Distance.

Table 2. Summary of Model Parameters and Accuracy

Model	Setting	Size(kb)	Error(mm)
RF	100 Trees,min samples split: 2,min samples leaf: 1	68234	11.32
SVR	RBF kernel,C=100,epsilon=0.1	987	7.53
NN	6 hidden layers,An average of 200 neurons per layer	810	5.02

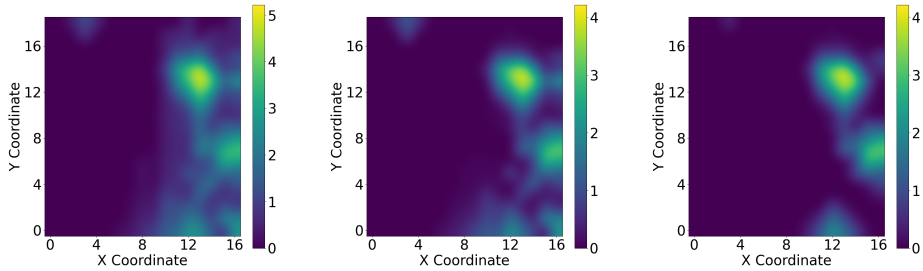

(a) RF (b) SVR (c) NN

Fig. 4. Localization Error(mm) of Different Models

This ensures that the corrections made to account for soft magnetic offsets are as precise as possible, leading to improved accuracy in the magnetic tracking system.

With this standard in place, we initially explored three fundamental machine learning approaches: linear regression, decision trees, and random forests. Remarkably, linear regression demonstrated optimal performance, achieving an tracking error of 8.32mm. This notable success motivated further investigation and subsequent model optimizations.

Despite marginal improvement with regularized linear models (Ridge and Lasso regression), reaching an error of around 7mm, our final experimentation introduced a multilayer perceptron neural network. This advanced model outperformed traditional linear approaches, achieving an impressive error of 5mm. Evaluation of the neural network's effectiveness continued to rely on the established Euclidean Distance metric.

4.2.2 Position Recognition and Model Integration. We utilize a dataset comprising four groups for training and one group for testing to assess the performance of three lightweight machine learning models: Random Forest (RF), Support Vector Regression (SVR) with a radial basis function (RBF) kernel and Neural Network (NN). The experimental setup and the model sizes are detailed in Table 2, while the average localization error is illustrated in Figure 4.

Evaluation includes measuring the inference time per sample on a desktop equipped with an Intel i5-12400F CPU.

All three models demonstrate an achievement of millimeter-level error in localization accuracy. Notably, the overhead of the Neural Network (NN) is observed to be more balanced compared to RF and SVR. Figure 10 visually represents that the error distribution of NN is more even across the dataset. Based on the findings, NN is selected as the machine learning model for tracking Mring using magnetic field strength.

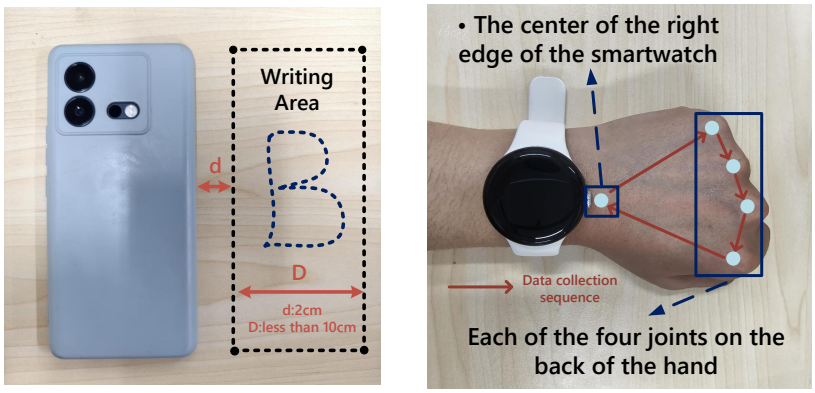

(a) Smart Phone (b) Smart Watch

Fig. 5. Data Collection on Different Platforms

In conclusion, the study demonstrates the suitability of Neural Network for accurate Mring tracking based on magnetic field strength, emphasizing the need for model retraining when there are changes in the device models involved.

4.2.3 Application of Transfer Learning. In the domain of transfer learning, our research focuses on expanding application scenarios and user features. Additionally, we address the segmentation of various subjects within these scenarios, such as human users and various hardware configurations. Leveraging pre-trained models from previous training sessions, we intend to adapt the system to these novel environments through a meticulous process.

The experimenters were instructed to pause at several strategically selected fixed positions to ensure comprehensive data collection. We used completely different feature extraction methods for smartphones and smartwatch platforms. However, the underlying reasons for these methods are the same: to effectively collect and utilize user interaction data with smart devices.

- **Personalized Hand Size Data:** These joints represent key anatomical points that produce personalized body data crucial to understanding user interactions with the smartwatch.
- **Usage Range Delineation:** By pausing at these fixed positions, we delineate the subsequent usage ranges of the smartwatch, facilitating a more nuanced analysis of user interactions and environmental effects.

In detail, experimenters are instructed to pause for 3 seconds at the following fixed positions.

Smartphone Platform: Due to the magnetometer of smartphones typically being located on the right side, its usage range is oriented towards the right side of the phone. As shown in Figure 5a, the user must define the usage range by determining four points within a rectangle. Specifically, these four points are:

- Two vertices on the right side of the phone, 2cm from the right edge.
- Any point to the right of the above two points, at a certain distance (not exceeding 10cm), determined by the user.

Smartwatch Platform: We assume that the input area of the smartwatch is the user's dorsal hand area where the smartwatch is worn. Therefore, as shown in Figure 5b, it's necessary to confirm the boundaries of the user's dorsal hand area, specifically:

- The center of the right edge of the smartwatch.
- Each of the four joints on the back of the hand, excluding the thumb.

This deliberate pause duration and position selection ensure a comprehensive sampling of data points that encapsulate various aspects of user interactions and environmental conditions. Additionally, it enables the subsequent fine-tuning and adaptation of the system to diverse usage scenarios encountered in airborne and underwater environments.

The initial phase of data preparation entails meticulous organization of the gathered data into a format tailored for training neural networks. Given that the data set comprises three-dimensional magnetic vector values (represented by x, y, and z coordinates), we integrate this information with corresponding environmental labels (e.g., "underwater" or "airborne") to form cohesive training samples.

Following this, we deliberately selected a pretrained neural network model to serve as our foundational framework. This model exhibits a robust capability to adapt to the intricacies of magnetic vector localization tasks, characterized by its depth, complexity, and inherent sensitivity to magnetic data.

In preparation for transfer learning, we meticulously loaded the chosen base model and embarked on a fine-tuning process. Here, we made a strategic decision to maintain the integrity of the majority of the base model's parameters while selectively adjusting parameters within its final layers. Furthermore, we leveraged automated tuning tools such as Grid Search to systematically explore optimal hyperparameter combinations, thereby enhancing the model's adaptability to novel environmental contexts and diverse datasets.

Subsequently, armed with the fine-tuned model, we proceeded to train our dataset, guiding the model to assimilate and comprehend the nuances present in the newly collected data. Following this training phase, we subjected the fine-tuned model to comprehensive performance evaluations, scrutinizing its efficacy and robustness in handling the designated localization task.

4.3 Model Distillation

A simplified student model is designed with careful consideration of the resource limitations inherent in smartwatches, which typically have significantly lower processing power and memory compared to smartphones[38]. To address these hardware constraints, we employed model distillation, a technique that allows us to transfer essential knowledge from a larger, more complex teacher model to a smaller, more efficient student model. This method not only reduces the size and complexity of the model but also ensures that the student model retains key performance characteristics, allowing it to operate effectively within the limited computational capacity of smartwatches.

By distilling the knowledge from the teacher model, we compress the critical information into the student model while maintaining an acceptable level of accuracy and efficiency. This approach is particularly beneficial for ensuring real-time operation on smartwatches, where resource constraints make running large, high-complexity models impractical. Compared to traditional transfer learning, which fine-tunes a pre-trained model without necessarily reducing its size, model distillation specifically targets reducing the model's computational and memory footprint, enabling the system to run efficiently on low-power devices without sacrificing essential performance. The basic process of model distillation is illustrated in Figure 6.

4.3.1 Teacher Model Training. We trained the model on the smartphone platform as the teacher model to validate the system design and collect data. We developed a dedicated smartphone application specifically for data collection and initial model training. As previously mentioned, data collection and processing occurred on smartphones, while subsequent teacher model training took

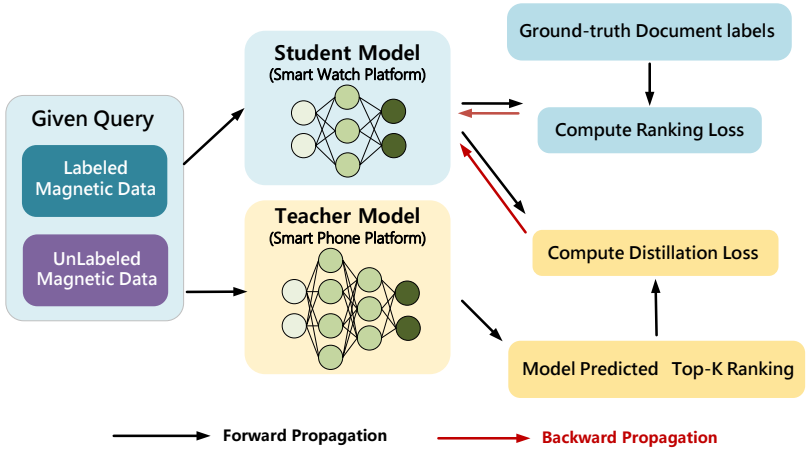

Fig. 6. Model Distillation

place on server infrastructure. The teacher model is a sophisticated neural network consisting of two independent parts, each with six hidden layers, trained using the collected data. The first part of the neural network processes raw input data to generate output used for further training in the second part.

4.3.2 Student Model Training. In this phase, the focus shifted towards the development and training of a simplified student model tailored to the resource constraints imposed by the smartwatch environment. The following steps were undertaken:

Designing a Simplified Student Model: A key aspect involved in this phase was the redesign of the student model to align with the limited computational resources available on smartwatches. Accordingly, the number of hidden layers was reduced to three, ensuring compatibility with the device's constraints.

Determining Distillation Loss Weight: To facilitate effective knowledge transfer from the teacher model to the student model, it was necessary to establish an appropriate weight for the distillation loss. This weight serves to balance the primary task loss with the similarity between the outputs of the teacher and student models. A weight of 0.5 was selected based on experimentation and empirical observations.

Training the Student Model: The training process involved using the output of the teacher model as an auxiliary target and integrating the distillation loss term into the overall loss function. Through this approach, the student model was trained to simultaneously learn the target task and assimilate the knowledge distilled from the teacher model.

Evaluating the Student Model: After training, the performance of the student model was evaluated to assess its efficacy and compare it with the teacher model. Notably, the student model had an error only about 1mm higher than the teacher model, and the overall trajectory pattern reconstruction was essentially consistent, demonstrating the effectiveness of the distillation process in transferring knowledge to a resource-constrained environment such as a smartwatch.

4.4 Trajectory Smoothing and User Input Processing

Algorithm 1 Trajectory Smoothing and User Input Processing

Require: Trajectory points T_p
Ensure: Smoothed trajectory T_s

for i from 1 to $length(T_p)$ **do**
  $current \leftarrow T_p[i]$
  $window \leftarrow T_p[i - \min(\text{window\_size}, i-1) : i]$
  $lof \leftarrow LOF(current, window)$
  if $lof > thre$ **then**
    $r \leftarrow 1$
    while $r \leq max$ **do**
      $window_s \leftarrow T_p[max(1, i-r) : \min(length(T_p), i+r)]$
      $point_s \leftarrow Average(window_s)$
      if $point_s == current$ **then**
        $T_s.append(point_s)$
        break
      else
        $lof_s \leftarrow LOF(point_s, window)$
        if $lof_s < lof$ **then**
          $T_s.append(point_s)$
          break
        else
          $r \leftarrow r + 1$
        end if
      end if
    end while
  else
    $T_s.append(current)$
  end if
end for
return T_s

After preprocessing the data, which resulted in obtaining the index of the user's input positions, the necessary step to obtain the final trajectory is trajectory smoothing, following the specific process outlined in Algorithm 1.

Algorithm 1 initially employs the Local Outlier Factor (LOF) [3] algorithm to detect outlier points on the trajectory. The LOF algorithm, based on local density estimation, excels at identifying points significantly deviating from their local neighborhoods. The local density of a data point can be defined as the sum of the reciprocals of the distances from its neighboring data points. A higher density indicates denser neighboring data points, while a lower density implies that the point resides in a relatively sparse region.

Considering the sequential nature of the trajectories, we utilized a sliding-window approach to compute the local density of each point. In particular, only the preceding points in the trajectory are considered neighbors when computing the local density. This selective consideration enables the algorithm to focus more on the immediate vicinity of each point, thereby mitigating the influence of the entire trajectory dataset.

When outlier points are detected, we apply data smoothing techniques, specifically the moving average method, to address them. The moving average algorithm operates by iteratively increasing

the radius of a moving window and computing the average within it. If the average remains unchanged upon increasing the radius, the current point is considered a valid result. However, if the average changes, we prioritize points with higher local density to ensure that the replacement maintains the integrity of the trajectory while minimizing the impact of outliers.

By adhering to the aforementioned steps outlined in Algorithm 1, we aim to achieve trajectory smoothing and improve the quality and usability of the trajectory data for further analysis and applications.

5 EVALUATIONS

In this section, we will specifically describe our experiments. We independently developed software for both mobile and watch platforms to collect data and calculate trajectories. We conducted multiple sets of experiments to ensure our system performs excellently under various inputs. Additionally, we performed numerous comparative experiments to demonstrate the effectiveness of our smoothing algorithm and model distillation. To evaluate robustness in different environments, we conducted tests under varying conditions and obtained satisfactory results. Finally, we collected usage data from 25 volunteers to test the stability of our system and user experience across multiple dimensions.

5.1 Implementation

We have implemented a prototype of Mring to validate its performance in 2D tracking and handwriting. To facilitate the use of optimizers and machine learning models, we have implemented Mring using a client-server architecture. We developed an application on the Android platform as well as the Android Wear platform that can collect magnetometer readings and provide calibration instructions. We set the magnetometer's sampling rate to 50 Hz, which means it collects 50 magnetic data points per second. We send this data to the PC platform for processing. Additionally, we have developed standalone software on the PC platform for real-time data reception, processing, and visualization. The default mobile device is the vivo X100 Pro, and the default smartwatch device is the Google Pixel Watch. During the initial run, we first define the area. Following the procedure in section four, we collect user's writing boundaries and environmental data through fixed steps for calibration. Afterward, we use a ring embedded with a strong magnet for writing.

5.2 Tracking on Smart Phone Platform

5.2.1 Set Up. We first prepared an A4 paper with a grid pattern to indicate position coordinates. The grid consists of 5 mm × 5 mm squares, making up a grid area of 16 cm × 10 cm, roughly matching the length and width of the test phone, in line with the region division strategy I introduced in section four. We calculate the coordinates of each grid square with the origin at the top-right vertex of the grid closest to the phone. The initial distance between the earpiece and the smartphone is 2 centimeters. Initially, we moved the ring in a serpentine pattern following the coordinate sequence, pausing for 2 seconds at each grid position to collect the relationship between grid position information and magnetic coordinates. Afterward, we traced the path on the paper's grid as ground truth, then moved the ring along the path at the same time intervals.

5.2.2 Tracking Result and Impact of Trajectory Smoothing. In our experimental setup, we strategically differentiated the speeds for data collection and user interaction to optimize the model's performance across various scenarios.

Data Collection Speed: We pre-drew the user's action trajectories and moved the ring with a strong magnet along these paths. To ensure comprehensive data collection, the ring was moved slowly along the path, pausing for approximately 1-2 seconds at each grid square. This deliberate

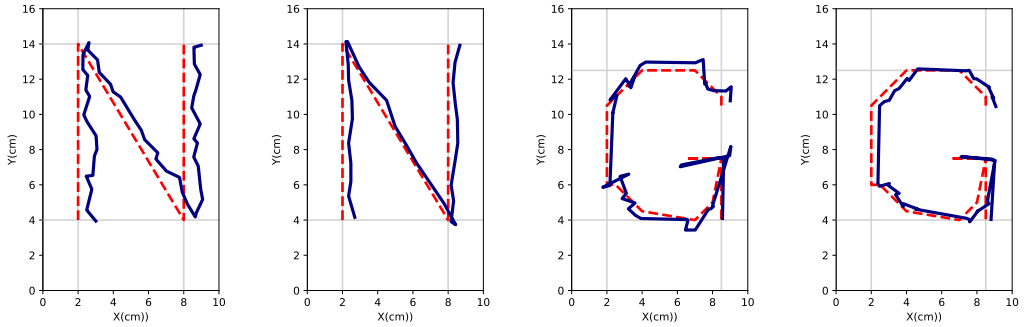

(a) 'N' Before Smoothing (b) 'N' After Smoothing (c) 'G' Before Smoothing (d) 'G' After Smoothing

Fig. 7. Trajectory Result on Smart Phone Platform

pacing was chosen to balance data accuracy. Moving the ring too swiftly (less than 1 second per grid square) would risk collecting insufficient data points, potentially leading to gaps in the signal that could diminish tracking precision. Conversely, overly lengthy pauses (more than 2 seconds) could cause the model to overfit to these slow movements, thereby reducing its ability to generalize to quicker, more natural user interactions.

User Interaction Speed: During actual user interaction, the model is designed to respond to more rapid movements, with users typically completing a stroke every second. This faster interaction speed challenges the model to adapt to the natural pace of user activities without compromising accuracy or responsiveness. These distinct speed settings are crucial for training the model under controlled, slow-motion conditions to capture detailed data, while also ensuring it performs effectively at the practical speed of real-world usage.

We conducted experiments on commonly used letters and numbers. However, to demonstrate the model's performance on straight and curved models, we selected letters 'N' and 'G' for presentation. As shown in Figure 7, the red dashed line represents the ground truth, while the solid line in deep blue represents the results recognized by the model. The two images depict the trajectories before and after being processed by the trajectory smoothing algorithm, aiming to showcase the effectiveness of the trajectory smoothing algorithm. We calculated the distance between each recognized point and the true coordinates as the error and determined the error interval and average error of the entire image recognition result.

For the letter 'N', its tracking error was 4.7mm, which decreased to 3.8mm after trajectory smoothing. For the letter 'G', its tracking error was 6.3mm, which reduced to 4.9mm after trajectory smoothing. Although the directly recognized results already resembled the original images, the error significantly decreased after trajectory smoothing, making the trajectories easier to recognize.

5.3 Tracking on Smart Watch Platform

5.3.1 Set Up. Due to the inconvenience of using the back of the hand for experiments, we also prepared an A4 paper with a grid pattern to indicate position coordinates. The grid size is 8 cm×8 cm, which aligns with the average size of the back of the hand writing area. Similarly, we use the top-left vertex of the grid as the origin to calculate the coordinates of each grid square and collect data, establishing the basic relationship between magnetic data and coordinates. Subsequent tuning and optimization will also be based on this. Afterward, we will follow the same procedure as with

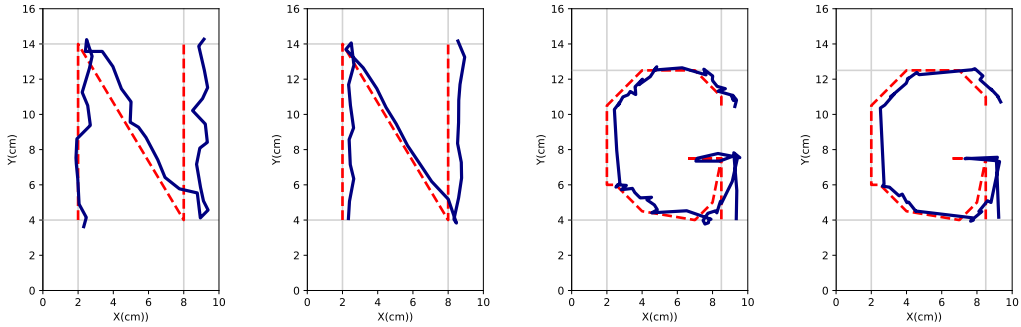

(a) 'N' Before Smoothing (b) 'N' After Smoothing (c) 'G' Before Smoothing (d) 'G' After Smoothing

Fig. 8. Trajectory Result on Smart Watch Platform

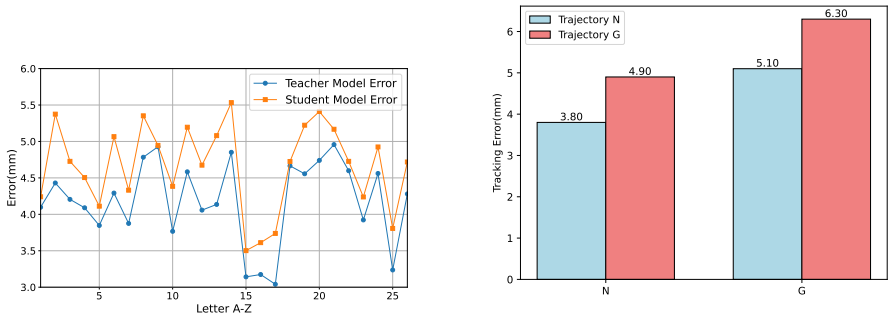

(a) The Results of All Cases (b) The Results of Special Cases

Fig. 9. The Effectiveness of Model Distillation

the mobile platform, tracing the path on the paper's grid as ground truth, then moving the ring along the path at the same time intervals.

5.3.2 Impact of Model Distillation. We trained both the teacher model and the student model with the same data, following an identical trajectory smoothing process. We first conducted experiments on the 26 English letters. Following the previous steps, we sequentially input the same collected experimental data into both the teacher model and the student model. The trajectory results are shown in Figure 8. As shown in Figure 9, the error of the student model slightly increased. Specifically, the average error for trajectory N increased from 3.8mm to 4.9mm, and for trajectory G, the average error increased from 5.1mm to 6.3mm. Although the errors increased, the overall trend remained unchanged, and the degree of trajectory restoration was similar. Additionally, the increased errors were within an acceptable range.

5.4 Comparative Analysis with Baseline Methods

We conduct a comparative analysis of our system against similar research employing analogous tracking configurations. TRing is selected as a baseline due to its use of a permanent magnet and a single magnetometer for calibration, which aligns with key elements of our system. Although

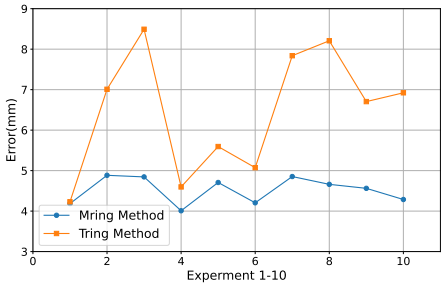

Fig. 10. Comparison of Tracking Error

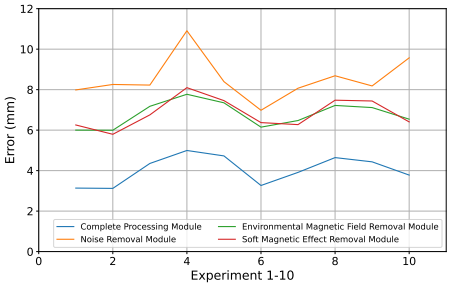

Fig. 11. Impact of Preprocessing Modules

TRing's configuration features a moving magnetometer and a stationary magnet, contrasting with the stationary magnetometer and moving magnet in our setup, the application context remains highly comparable. Moreover, the data processing techniques utilized in TRing provide a robust foundation for evaluating the performance of our method, making it an appropriate benchmark for this study.

To evaluate the performance of our system, we processed the same set of 10 data samples using both our proposed method and the method outlined in TRing. The resulting positioning errors for these samples are depicted in Figure 10, where we present the average error for each method. On average, our approach achieved approximately 2 mm higher precision compared to TRing's method, demonstrating a notable improvement in accuracy.

5.5 The Impact of Different Preprocessing Modules

To evaluate the impact of preprocessing modules on positioning accuracy, we conducted ablation tests. These tests quantify the contribution of each preprocessing step by systematically removing it. The following modules were tested:

Noise Reduction Module: We removed the Kalman filter and directly used raw magnetic field data for positioning. By comparing the positioning accuracy with and without the noise reduction processing, we assess the effect of the noise reduction module on positioning accuracy.

Elimination of Static Magnetic Field in Environmental Magnetic Fields: In this test, we removed the static magnetic field elimination processing and used unadjusted magnetic field data directly for positioning. We compared the positioning accuracy before and after removing the static magnetic field processing to evaluate its necessity.

Elimination of Soft Magnetic Effects in Environmental Magnetic Fields: We removed the soft magnetic effect elimination processing and used unprocessed magnetic field data directly for positioning. By comparing the positioning accuracy before and after removing the soft magnetic effect processing, we assess the impact of this step on positioning accuracy.

The results of these ablation tests are illustrated in the Figure 11. These figures clearly show the impact of each preprocessing module on positioning accuracy. Notably, removing the Noise Reduction Module resulted in the largest increase in error, with the error rising by approximately 5 mm—double the original error—which made it impossible to recognize the image as a discernible shape. Similarly, the removal of the Environmental Magnetic Field Correction and Soft Magnetic Effect Removal modules both caused the error to increase by about 3 mm, representing a 75% increase in error. This is also an unacceptable level of degradation, further underscoring the critical role each preprocessing stage plays in ensuring accurate positioning.

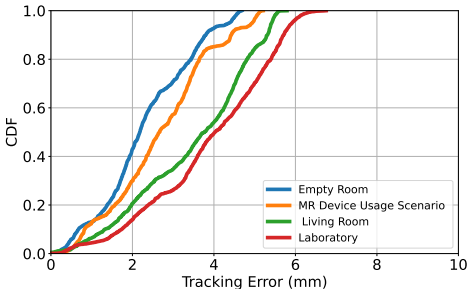

Fig. 12. Impact of Different Environments

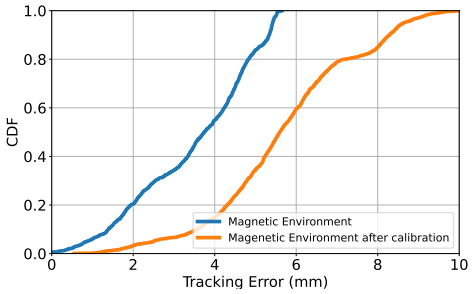

Fig. 13. Impact of Soft Iron Calibration

Table 3. Comparison of Device Models, Processors, and Battery Capacity

Device Model	Processor	Battery Capacity (mAh)
vivo X100 pro	MediaTek Dimensity 9300	5400
IQOO neo 3	Snapdragon 865	4500
HUAWEI MATE 20	Kirin 980	4000
OPPO Realme GT neo5	Snapdragon 8+ Gen1 (underclocked)	4600
IQOO 11	Snapdragon 8 Gen2	5000

5.6 Impact of Magnetic Interference

The magnetic interference in the surrounding environment is a crucial issue that must be addressed. We conducted experiments in multiple environments. Initially, we conducted experiments in an empty classroom using a wooden desk without ferrous supports as the support platform, considering it as ground truth. Following this, we tested in various scenarios such as a living room equipped with various electronic furniture, a laboratory with numerous computers and monitors, and additionally, we simulated usage scenarios by placing an active MR device next to the experimental platform. In order to demonstrate the effectiveness of our soft magnetic correction algorithm, we placed a strong magnet on the table, considering it as a strong magnetic environment. During data processing, we trained the models with both the data corrected by the soft magnetic correction algorithm and the uncorrected data.

As shown in the Figure 12, the Mring program achieved relatively excellent results in several everyday environments: the laboratory, the living room, and the MR usage environment. Their average errors were 3.51mm, 4.77mm, and 4.91mm, respectively. Compared to the error of 2.81mm in the clean room, the increase in errors in the other environments is within an acceptable range. For performance in a strong magnetic environment, we conducted recognition using data that had not undergone soft magnetic correction training and compared it with the recognition results using data that had undergone soft magnetic correction. As shown in the Figure 13, the final results showed a reduction in error of nearly 3mm. This is sufficient to demonstrate the reliability of the soft magnetic correction function.

5.7 Energy Overhead

To evaluate the power consumption and task execution time of the Mring system across different devices, we conducted controlled experiments, ensuring consistent testing conditions.

Since the devices have different battery capacities, we calculated the battery drop as a percentage of the total capacity to standardize comparisons. The battery percentage drop during each test was converted into mAh, allowing for a fair comparison of power consumption across devices. To further clarify the experimental settings and single out Mring's impact on energy consumption, during the entire data collection process of our experiment, we took strict measures to ensure that there were absolutely no other programs running in the background of the experimental device. Only the data collection program dedicated to our study was in operation. Additionally, to accurately calculate the power consumption solely attributable to Mring, we collected the power consumption of the device with the screen on but without running any programs within the same time range as the data collection for Mring. Then, we subtracted this value from the power consumption recorded during the Mring experiment to precisely obtain the power consumption data of our program.

A table summarizing the key specifications for each device, including processor type, battery capacity, and test conditions, is provided in Table 3.

After performing calibration and drawing operations for 1 minute, the actual power consumption across different devices varied notably. Specifically, the vivo X100 Pro consumed 2% of its battery, which is equivalent to 108mAh. The IQOO neo 3 consumed 10% of its battery, which is equivalent to 450mAh. The HUAWEI MATE 20 consumed 12% of its battery, which is equivalent to 480mAh. The OPPO Realme GT neo5 consumed 8% of its battery, which is equivalent to 368mAh. The IQOO 11 consumed 4% of its battery, which is equivalent to 200mAh. These results demonstrate a clear relationship between the power consumption and the processing power of each device. Smartphones with more advanced processors, such as the MediaTek Dimensity 9300 (vivo X100 pro) and Snapdragon 8 Gen2 (IQOO 11), showed significantly lower power consumption, suggesting that these devices are more efficient in handling the operations required by the Mring system. On the other hand, devices with older or less efficient processors, such as the Kirin 980 (HUAWEI MATE 20) and Snapdragon 865 (IQOO neo 3), exhibited higher power usage.

Despite these variations, the overall power consumption of our system remains within acceptable limits across all devices. This indicates that the Mring system is optimized for a range of hardware configurations, maintaining efficiency and stability, even on devices with less advanced processors. These findings further underscore the adaptability and practicality of the system, ensuring a balance between computational performance and energy efficiency.

Specifically, we measured and compared the error of each device when using the Mring system. As shown in the Figure 14, the experimental results showed that the average error for the vivo X100 pro was 3.55 mm, for the IQOO neo 3 it was 5.12 mm, for the HUAWEI MATE 20 it was 5.22 mm, for the OPPO Realme GT neo5 it was 4.96 mm, and for the IQOO 11 it was 3.56 mm. These data indicate that despite differences in hardware configurations and magnetic sensor performance among different devices, the Mring system can still maintain high accuracy and reliability across all devices.

The experimental results demonstrate that the Mring system has good device adaptability, capable of achieving stable non-contact input functionality on a variety of smartphone models. This further proves the universality and practicality of our proposed magnetic signal sensing technology.

5.8 User Study

To comprehensively evaluate the performance of the Mring system, we conducted detailed experiments involving 25 volunteers. We recorded the time taken for calibrating data, the trajectory reconstruction error, and the users' preference for the system. These 25 volunteers first conducted tests on a smartphone platform, followed by tests on a smartwatch platform. During the experiments, the volunteers were asked to perform parameter calibration according to a predefined calibration method, then perform trajectory recognition, and finally record the results.

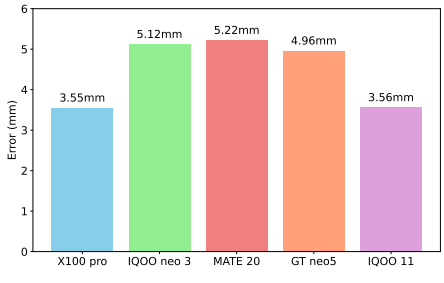

Fig. 14. Impact of Different Devices

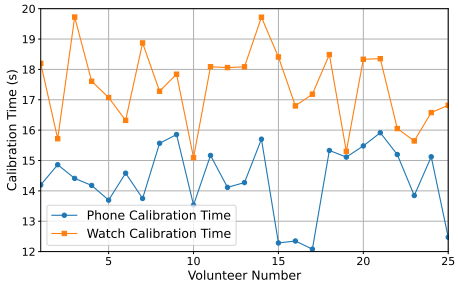

Fig. 15. Calibration Time of 25 Volunteers

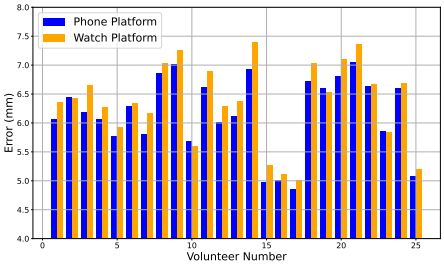

Fig. 16. Tracking Error of 25 Volunteers

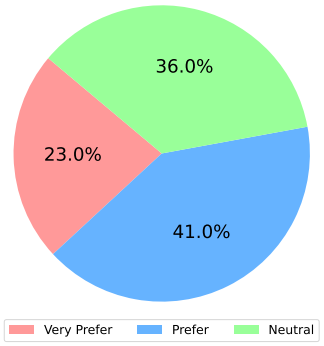

Fig. 17. User Preference of Mring

The experimental results are shown in Figure 15: the calibration time on the smartphone platform was significantly less than the calibration time on the smartwatch platform. This difference is mainly due to the different number of vertices that need to be determined. On the smartphone platform, the larger screen allows users to complete the calibration process more quickly; on the smartwatch platform, the smaller screen requires more time to accurately determine the calibration vertices.

Regarding trajectory error, as shown in the Figure 16, the experimental data showed that the errors on the smartphone and smartwatch platforms were similar, with the smartwatch platform having a slightly larger error than the smartphone platform. This is likely due to the limited display and operation space on the smartwatch platform, causing a slight decrease in accuracy during trajectory recognition.

Finally, we conducted a survey to assess the users' acceptance of the Mring system. As shown in Figure 17, the survey results showed that 23% of the users were very satisfied with the system (very prefer), 41% of the users were satisfied (prefer), and the remaining users were neutral. These feedback results indicate that, despite some platform differences, the majority of users had a positive attitude towards the overall performance and user experience of the Mring system.

6 LIMITATIONS

One major limitation of our magnetic field sensing and localization system is its sensitivity to continuous and severe variations in the background magnetic field. In real-world environments, particularly urban or industrial settings, the magnetic field can be highly dynamic due to various sources such as electrical equipment, vehicles, and magnetic structural elements. These fluctuations introduce substantial noise, interfering with the precise detection of magnetic field changes caused by the target. Additionally, our system is susceptible to interference from other targets. If multiple users are using the system simultaneously, significant disturbances can occur. Unlike modulated electromagnetic signals, the raw magnetic signals cannot distinguish between the actions of different users. Currently, we are unable to distinguish the movements of multiple magnets.

7 CONCLUSION

In this study, we introduced Mring, a novel non-contact extended input method based on magnetic signals for MR and AR devices. By leveraging low-cost permanent magnets and existing magnetometer sensors in wearable devices, we developed a system capable of achieving high-precision localization and trajectory recognition, even outside the direct line of sight. Our research tackled significant challenges, including electromagnetic interference and user/scene adaptation. We employed noise filtering and a magnetic dipole model to stabilize and process magnetic signals, and trained neural networks to handle soft magnetic offsets. Our trajectory reconstruction accuracy is approximately 5.23mm. On the smartphone platform, the average error can be reduced to around 4.55mm, while on the smartwatch platform, it is approximately 7.02mm. The performance of our system was validated through experiments in various environments, demonstrating its robustness and adaptability.

Moreover, we addressed the diversity of scenarios by developing a comprehensive calibration approach and optimizing computational costs for smartwatches using model distillation techniques. Our innovative input method enhances user interaction with MR and AR technologies, providing a reliable and efficient solution for diverse application scenarios.

In conclusion, Mring represents a significant advancement in the field of MR and AR interactions, offering a practical and effective solution for non-contact input based on magnetic signals. Future work will focus on further improving the system's adaptability and exploring additional applications of this technology in different domains.

8 ACKNOWLEDGMENTS

This research was funded by the National Natural Science Foundation of China grant No. 62272427, 62072278 and U23A20273, the Hainan Provincial Joint Project of Sanya Yazhou Bay Science and Technology City No. 2021JJLH0060 and the Shandong Provincial Youth Innovation Team 2022KJ043, the Shandong Provincial Natural Science Foundation under Grant ZR2022LZH010, and the Taishan Scholars Program.

REFERENCES

[1] Takehiro Abe and Daisuke Sakamoto. 2021. MagneTrack: Magnetic Field Separation Method for Continuous and Simultaneous 1-DOF Tracking of Two-magnets. In *Proceedings of the 23rd International Conference on Mobile Human-Computer Interaction* (Toulouse & Virtual, France) *(MobileHCI '21)*. Association for Computing Machinery, New York, NY, USA, Article 1, 11 pages. https://doi.org/10.1145/3447526.3472052

[2] Fadel Adib, Zachary Kabelac, Dina Katabi, and Robert C. Miller. 2014. 3D tracking via body radio reflections. In *Proceedings of the 11th USENIX Conference on Networked Systems Design and Implementation* (Seattle, WA) *(NSDI'14)*. USENIX Association, USA, 317–329.

[3] Markus M. Breunig, Hans-Peter Kriegel, Raymond T. Ng, and Jörg Sander. 2000. LOF: identifying density-based local outliers. In *Proceedings of the 2000 ACM SIGMOD International Conference on Management of Data* (Dallas, Texas, USA)

(SIGMOD '00). Association for Computing Machinery, New York, NY, USA, 93–104. https://doi.org/10.1145/342009.335388

[4] Xudong Cai, Yongcai Wang, Zhe Huang, Yu Shao, and Deying Li. 2024. VOLoc: Visual Place Recognition by Querying Compressed Lidar Map. arXiv:2402.15961 [cs.CV] https://arxiv.org/abs/2402.15961

[5] Dongyao Chen, Mingke Wang, Chenxi He, Qing Luo, Yasha Iravantchi, Alanson Sample, Kang G. Shin, and Xinbing Wang. 2021. MagX: wearable, untethered hands tracking with passive magnets. In *Proceedings of the 27th Annual International Conference on Mobile Computing and Networking* (New Orleans, Louisiana) *(MobiCom '21)*. Association for Computing Machinery, New York, NY, USA, 269–282. https://doi.org/10.1145/3447993.3483260

[6] Ke-Yu Chen, Shwetak N. Patel, and Sean Keller. 2016. Finexus: Tracking Precise Motions of Multiple Fingertips Using Magnetic Sensing. In *Proceedings of the 2016 CHI Conference on Human Factors in Computing Systems* (San Jose, California, USA) *(CHI '16)*. Association for Computing Machinery, New York, NY, USA, 1504–1514. https://doi.org/10.1145/2858036.2858125

[7] Sneha Das and Sonali Vyas. 2023. The Utilization of AR/VR in Robotic Surgery: A Study. In *Proceedings of the 4th International Conference on Information Management & Machine Intelligence* (Jaipur, India) *(ICIMMI '22)*. Association for Computing Machinery, New York, NY, USA, Article 61, 8 pages. https://doi.org/10.1145/3590837.3590898

[8] Anthony Paul Franze, Glenda Amayo Caldwell, Muge Fialho Leandro Alves Teixeira, and Markus Rittenbruch. 2023. Employing AR/MR Mockups to Imagine Future Custom Manufacturing Practices. In *Proceedings of the 34th Australian Conference on Human-Computer Interaction* (Canberra , ACT, Australia) *(OzCHI '22)*. Association for Computing Machinery, New York, NY, USA, 206–215. https://doi.org/10.1145/3572921.3576201

[9] Ruiyang Gao, Mi Zhang, Jie Zhang, Yang Li, Enze Yi, Dan Wu, Leye Wang, and Daqing Zhang. 2021. Towards Position-Independent Sensing for Gesture Recognition with Wi-Fi. *Proc. ACM Interact. Mob. Wearable Ubiquitous Technol.* 5, 2, Article 61 (jun 2021), 28 pages. https://doi.org/10.1145/3463504

[10] Kyungjun Lee, Hong Li, Muhammad Rizky Wellyanto, Yu Jiang Tham, Andrés Monroy-Hernández, Fannie Liu, Brian A. Smith, and Rajan Vaish. 2023. Exploring Immersive Interpersonal Communication via AR. *Proc. ACM Hum.-Comput. Interact.* 7, CSCW1, Article 50 (apr 2023), 25 pages. https://doi.org/10.1145/3579483

[11] Xinyi Li, Liqiong Chang, Fangfang Song, Ju Wang, Xiaojiang Chen, Zhanyong Tang, and Zheng Wang. 2021. CrossGR: Accurate and Low-cost Cross-target Gesture Recognition Using Wi-Fi. *Proc. ACM Interact. Mob. Wearable Ubiquitous Technol.* 5, 1, Article 21 (mar 2021), 23 pages. https://doi.org/10.1145/3448100

[12] Jess McIntosh, Paul Strohmeier, Jarrod Knibbe, Sebastian Boring, and Kasper Hornbæk. 2019. Magnetips: Combining Fingertip Tracking and Haptic Feedback for Around-Device Interaction. In *Proceedings of the 2019 CHI Conference on Human Factors in Computing Systems* (Glasgow, Scotland Uk) *(CHI '19)*. Association for Computing Machinery, New York, NY, USA, 1–12. https://doi.org/10.1145/3290605.3300638

[13] Yōko Miyatake, Rong-Hao Liang, Bing-Yu Chen, and Itiro Siio. 2021. FieldSweep: A 2D Tracking System With Embedded Magnets and a Smartphone. In *Extended Abstracts of the 2021 CHI Conference on Human Factors in Computing Systems* (Yokohama, Japan) *(CHI EA '21)*. Association for Computing Machinery, New York, NY, USA, Article 215, 6 pages. https://doi.org/10.1145/3411763.3451841

[14] Rajalakshmi Nandakumar, Vikram Iyer, Desney Tan, and Shyamnath Gollakota. 2016. FingerIO: Using Active Sonar for Fine-Grained Finger Tracking. In *Proceedings of the 2016 CHI Conference on Human Factors in Computing Systems* (San Jose, California, USA) *(CHI '16)*. Association for Computing Machinery, New York, NY, USA, 1515–1525. https://doi.org/10.1145/2858036.2858580

[15] Miyo Okada, Laura Lugaresi, Dingding Zheng, Roshan Peiris, Katrin Wolf, Cristian Norlin, Mikael Anneroth, Kai Kunze, and Masa Inakage. 2018. AURA: Urban Personal Projection to Initiate the Communication. In *Proceedings of the 2018 ACM International Conference on Interactive Surfaces and Spaces* (Tokyo, Japan) *(ISS '18)*. Association for Computing Machinery, New York, NY, USA, 397–399. https://doi.org/10.1145/3279778.3281758

[16] Ren Pingxuan. 2020. AR 3D Magic Book: A Healthy Interactive Reading Device Based on AR and Portable Projection. In *Proceedings of the 2020 International Conference on Computers, Information Processing and Advanced Education* (Ottawa, ON, Canada) *(CIPAE 2020)*. Association for Computing Machinery, New York, NY, USA, 244–250. https://doi.org/10.1145/3419635.3419714

[17] Qifan Pu, Sidhant Gupta, Shyamnath Gollakota, and Shwetak Patel. 2013. Whole-home gesture recognition using wireless signals. In *Proceedings of the 19th Annual International Conference on Mobile Computing & Networking* (Miami, Florida, USA) *(MobiCom '13)*. Association for Computing Machinery, New York, NY, USA, 27–38. https://doi.org/10.1145/2500423.2500436

[18] Qiang Qu, Hanxue Liang, Xiaoming Chen, Yuk Ying Chung, and Yiran Shen. 2024. NeRF-NQA: No-Reference Quality Assessment for Scenes Generated by NeRF and Neural View Synthesis Methods. *IEEE Transactions on Visualization and Computer Graphics* 30, 5 (2024), 2129–2139. https://doi.org/10.1109/TVCG.2024.3372037

[19] Iulian Radu, Tugce Joy, and Bertrand Schneider. 2021. Virtual Makerspaces: Merging AR/VR/MR to Enable Remote Collaborations in Physical Maker Activities. In *Extended Abstracts of the 2021 CHI Conference on Human Factors in*

Computing Systems (Yokohama, Japan) *(CHI EA '21)*. Association for Computing Machinery, New York, NY, USA, Article 202, 5 pages. https://doi.org/10.1145/3411763.3451561

[20] Anke Verena Reinschluessel, Thomas Muender, Roland Fischer, Valentin Kraft, Verena Nicole Uslar, Dirk Weyhe, Andrea Schenk, Gabriel Zachmann, Tanja Döring, and Rainer Malaka. 2023. Versatile Immersive Virtual and Augmented Tangible OR – Using VR, AR and Tangibles to Support Surgical Practice. In *Extended Abstracts of the 2023 CHI Conference on Human Factors in Computing Systems* (Hamburg, Germany) *(CHI EA '23)*. Association for Computing Machinery, New York, NY, USA, Article 477, 5 pages. https://doi.org/10.1145/3544549.3583895

[21] Gabriel Reyes, Jason Wu, Nikita Juneja, Maxim Goldshtein, W. Keith Edwards, Gregory D. Abowd, and Thad Starner. 2018. SynchroWatch: One-Handed Synchronous Smartwatch Gestures Using Correlation and Magnetic Sensing. *Proc. ACM Interact. Mob. Wearable Ubiquitous Technol.* 1, 4, Article 158 (jan 2018), 26 pages. https://doi.org/10.1145/3161162

[22] Ryo Shirai, Yuichi Itoh, and Masanori Hashimoto. 2021. Make it Trackable: An Instant Magnetic Tracking System With Coil-Free Tiny Trackers. *IEEE Access* PP, 99 (2021), 1–1.

[23] Yuka Tashiro, Shio Miyafuji, Yusuke Kojima, Satoshi Kiyofuji, Taichi Kin, Takeo Igarashi, and Hideki Koike. 2024. MR Microsurgical Suture Training System with Level-Appropriate Support. In *Proceedings of the CHI Conference on Human Factors in Computing Systems* (Honolulu, HI, USA) *(CHI '24)*. Association for Computing Machinery, New York, NY, USA, Article 460, 19 pages. https://doi.org/10.1145/3613904.3642324

[24] Klen Čopič Pucihar, Nuwan T. Attygalle, Matjaz Kljun, Christian Sandor, and Luis A. Leiva. 2022. Solids on Soli: Millimetre-Wave Radar Sensing through Materials. *Proc. ACM Hum.-Comput. Interact.* 6, EICS, Article 156 (June 2022), 19 pages. https://doi.org/10.1145/3532212

[25] Lihao Wang, Wei Wang, Haipeng Dai, and Shizhe Liu. 2023. MagSound: Magnetic Field Assisted Wireless Earphone Tracking. *Proc. ACM Interact. Mob. Wearable Ubiquitous Technol.* 7, 1, Article 33 (mar 2023), 32 pages. https://doi.org/10.1145/3580889

[26] Penghao Wang, Ruobing Jiang, Jingyang Hu, Yanmin Zhu, Hongbo Jiang, Minglu Li, and Chao Liu. 2024. AMT$^+$: Acoustic Multi-Target Tracking With Smartphone MIMO System. *IEEE Transactions on Mobile Computing* (2024), 1–16. https://doi.org/10.1109/TMC.2024.3417474

[27] Penghao Wang, Ruobing Jiang, Chao Liu, and Jun Luo. 2024. AGR: Acoustic Gait Recognition Using Interpretable Micro-Range Profile. In *IEEE INFOCOM 2024 - IEEE Conference on Computer Communications*. 1201–1210. https://doi.org/10.1109/INFOCOM52122.2024.10621283

[28] Wei Wang, Alex X. Liu, and Ke Sun. 2016. Device-free gesture tracking using acoustic signals. In *Proceedings of the 22nd Annual International Conference on Mobile Computing and Networking* (New York City, New York) *(MobiCom '16)*. Association for Computing Machinery, New York, NY, USA, 82–94. https://doi.org/10.1145/2973750.2973764

[29] Yanwen WANG, Jiaxing SHEN, and Yuanqing ZHENG. 2022. Push the Limit of Acoustic Gesture Recognition. *IEEE Transactions on Mobile Computing* 21, 5 (May 2022), 1798–1811. https://doi.org/10.1109/TMC.2020.3032278 The authors would like to thank the editor and reviewers for their help and insightful comments. This work was supported in part by the National Nature Science Foundation of China under grant 61702437 and Hong Kong GRF under Grant PolyU 152165/19E, and the Fundamental Research Funds for the Central Universities 531118010612..

[30] Yanxiang Wang, Xian Zhang, Yiran Shen, Bowen Du, Guangrong Zhao, Lizhen Cui, and Hongkai Wen. 2022. Event-Stream Representation for Human Gaits Identification Using Deep Neural Networks. *IEEE Transactions on Pattern Analysis and Machine Intelligence* 44, 7 (2022), 3436–3449. https://doi.org/10.1109/TPAMI.2021.3054886

[31] Teng Wei and Xinyu Zhang. 2015. mTrack: High-Precision Passive Tracking Using Millimeter Wave Radios. In *Proceedings of the 21st Annual International Conference on Mobile Computing and Networking* (Paris, France) *(MobiCom '15)*. Association for Computing Machinery, New York, NY, USA, 117–129. https://doi.org/10.1145/2789168.2790113

[32] Jon Whittle and Johann Schumann. 2004. Automating the implementation of Kalman filter algorithms. *ACM Trans. Math. Softw.* 30, 4 (dec 2004), 434–453. https://doi.org/10.1145/1039813.1039816

[33] Xiangwen Xiong and Wei Li. 2016. Antigravity and following VR, AR & MR system for spatial interaction. In *SIGGRAPH ASIA 2016 Posters* (Macau) *(SA '16)*. Association for Computing Machinery, New York, NY, USA, Article 9, 2 pages. https://doi.org/10.1145/3005274.3005326

[34] Zhaopeng Xu, Tong Liu, Ruobing Jiang, Pengfei Hu, Zhongwen Guo, and Chao Liu. 2024. AFace: Range-flexible Anti-spoofing Face Authentication via Smartphone Acoustic Sensing. *Proc. ACM Interact. Mob. Wearable Ubiquitous Technol.* 8, 1, Article 26 (March 2024), 33 pages. https://doi.org/10.1145/3643510

[35] Sang Ho Yoon, Yunbo Zhang, Ke Huo, and Karthik Ramani. 2016. TRing: Instant and Customizable Interactions with Objects Using an Embedded Magnet and a Finger-Worn Device. In *Proceedings of the 29th Annual Symposium on User Interface Software and Technology* (Tokyo, Japan) *(UIST '16)*. Association for Computing Machinery, New York, NY, USA, 169–181. https://doi.org/10.1145/2984511.2984529

[36] Sangki Yun, Yi-Chao Chen, Huihuang Zheng, Lili Qiu, and Wenguang Mao. 2017. Strata: Fine-Grained Acoustic-based Device-Free Tracking. In *Proceedings of the 15th Annual International Conference on Mobile Systems, Applications, and Services* (Niagara Falls, New York, USA) *(MobiSys '17)*. Association for Computing Machinery, New York, NY, USA,

15–28. https://doi.org/10.1145/3081333.3081356

[37] Marwa Zamali, Mohamed Latrach, Lotfi Osman, and Hedi Raggad. 2017. Study of meander dipole antenna coupled with magnetic metamaterial cells for UHF RFID system. In *Proceedings of the 2nd International Conference on Computing and Wireless Communication Systems* (Larache, Morocco) *(ICCWCS'17)*. Association for Computing Machinery, New York, NY, USA, Article 59, 5 pages. https://doi.org/10.1145/3167486.3167548

[38] Linna Zhang, Yuehui Chen, Yi Cao, and Yaou Zhao. 2023. BERT Model Compression With Decoupled Knowledge Distillation And Representation Learning. In *Proceedings of the 4th International Conference on Advanced Information Science and System* (Sanya, China) *(AISS '22)*. Association for Computing Machinery, New York, NY, USA, Article 16, 4 pages. https://doi.org/10.1145/3573834.3574482

[39] Suhong Zhang. 2022. PCB Design of Rogowski Coil with Strong Anti-Electromagnetic Interference. In *Proceedings of the 3rd Asia-Pacific Conference on Image Processing, Electronics and Computers* (Dalian, China) *(IPEC '22)*. Association for Computing Machinery, New York, NY, USA, 478–485. https://doi.org/10.1145/3544109.3544194

[40] Tongyu Zhang, Yiran Shen, Guangrong Zhao, Lin Wang, Xiaoming Chen, Lu Bai, and Yuanfeng Zhou. 2024. SwiftEye: Towards Anti-blink Pupil Tracking for Precise and Robust High-Frequency Near-Eye Movement Analysis with Event Cameras. *IEEE Transactions on Visualization and Computer Graphics* 30, 5 (2024), 2077–2086. https://doi.org/10.1109/TVCG.2024.3372039

[41] Guangrong Zhao, Yiran Shen, Ning Chen, Pengfei Hu, Lei Liu, and Hongkai Wen. 2024. EV-Tach: A Handheld Rotational Speed Estimation System With Event Camera. *IEEE Transactions on Mobile Computing* 23, 6 (2024), 7483–7498. https://doi.org/10.1109/TMC.2023.3335221